Poster P1.30

LABORATORY MEASURED ICE CRYSTAL CAPACITANCES & MASS DIMENSIONAL RELATIONS

Matthew Bailey and John Hallett

Introduction

Recent comprehensive laboratory and field studies have clarified many of the details concerning atmospheric ice crystal habits as a function of temperature, ice supersaturation, vapor diffusivity, and growth history (Bailey and Hallett, 2009). The picture revealed is one of a complexity of shapes that dominate habit distributions. From the laboratory study (Bailey and Hallett, 2004 = BH04) linear or maximum dimension growth rates, in addition to projected area and volume (mass) growth rates have been measured. However, these results have yet to be applied to cloud models by the modeling community, most likely due to reservations concerning their accuracy. In situ habit and size distributions have been extensively measured, but there is little temporal data available concerning the growth rates of in situ ice crystals with which laboratory measurements can be compared. One exception is the INTACC study of Field et al. (2001 = FE01) where ice crystal sizes were measured and growth times determined for a well characterized wave cloud case. Remarkable agreement is observed, confirming the reliability and applicability of the laboratory measurements obtained under simulated atmospheric conditions.

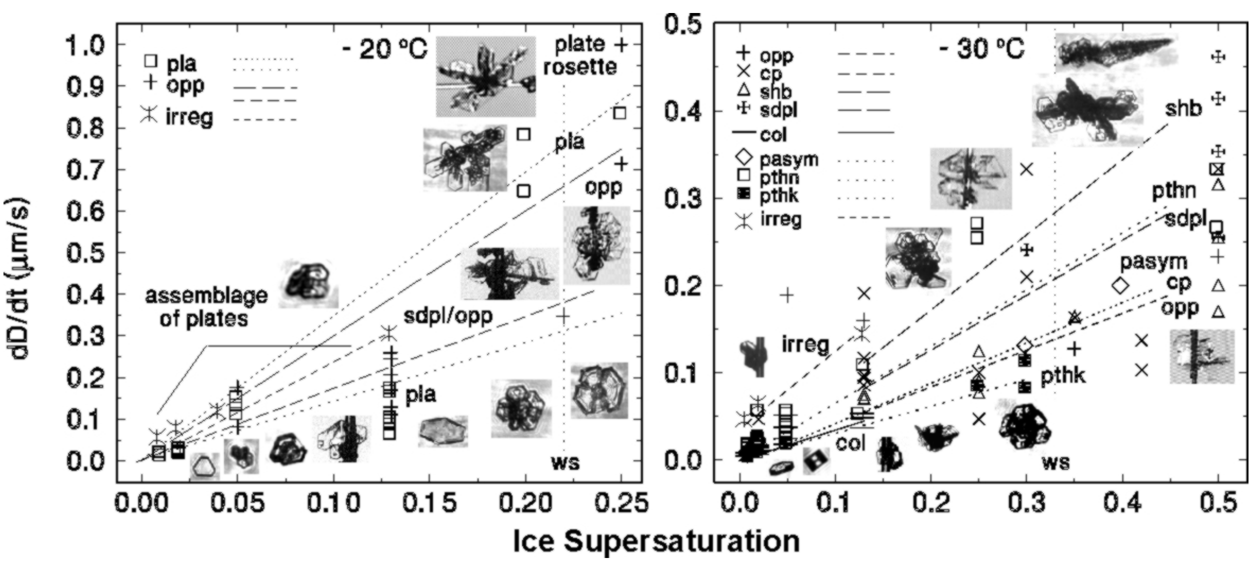

Figure 1. Laboratory measured ice crystal growth rates at -20 °C and -30 °C. Polycrystalline forms dominate the habit distribution at these temperatures, especially near water saturation (ws), indicated by the vertical dotted line in each graph. The fastest growing habits near water saturation are plate rosettes, side planes (sdpl), overlapping parallel plates (opp), irregular assemblages of plates, and compact faceted polyhedrons (irreg).

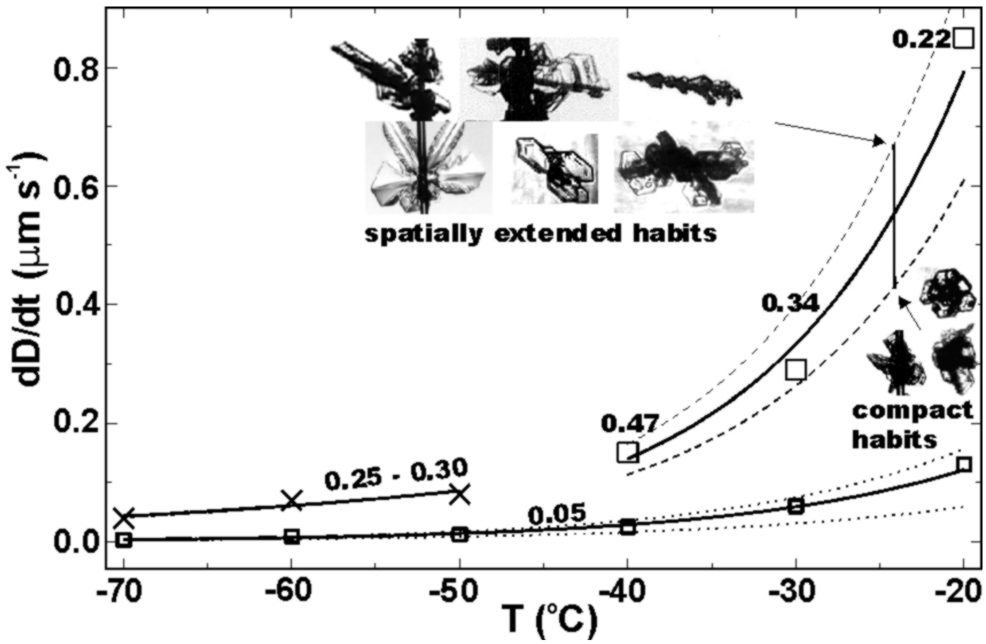

Figure 2. Exponential fits of average linear growth rates (habit weighted) as a function of temperature for some typical in situ ice supersaturations. Symbols and solid lines indicate the fits of the average values, while dashed and dotted lines represent the maximum and minimum rates. Decimal ice supersaturations equivalent to water saturation are indicated for temperatures between -20 °C and -40 °C, with values at temperatures ≤ - 50 °C indicative of typical cirrus ice supersaturations. The vertical line at -24 °C indicates the growth values used for comparison with the INTACC case of Field et al. (2001). Note that unventilated growth rates just below -20 °C approach 1 μm s^{-1}, in agreement with recent in situ observations of ventilated crystals by Heymsfield et. al (2010, this conference).

INTACC Comparison

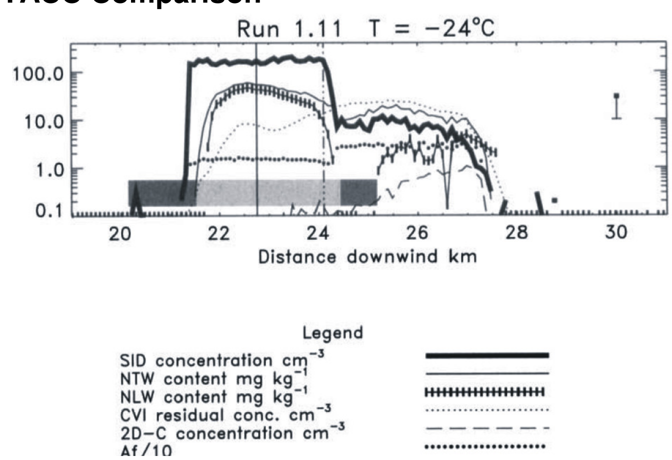

Figure 3. Instrument measurements of the INTACC wave cloud analyzed in this study similar to the one shown at right. Long dashed line at the bottom of the figure (beginning at about 23.5 km downwind) indicates ice crystal detection by a 2D-C probe at an assumed threshold size of approximately 25 micrometers near 23.5 km downwind distance.

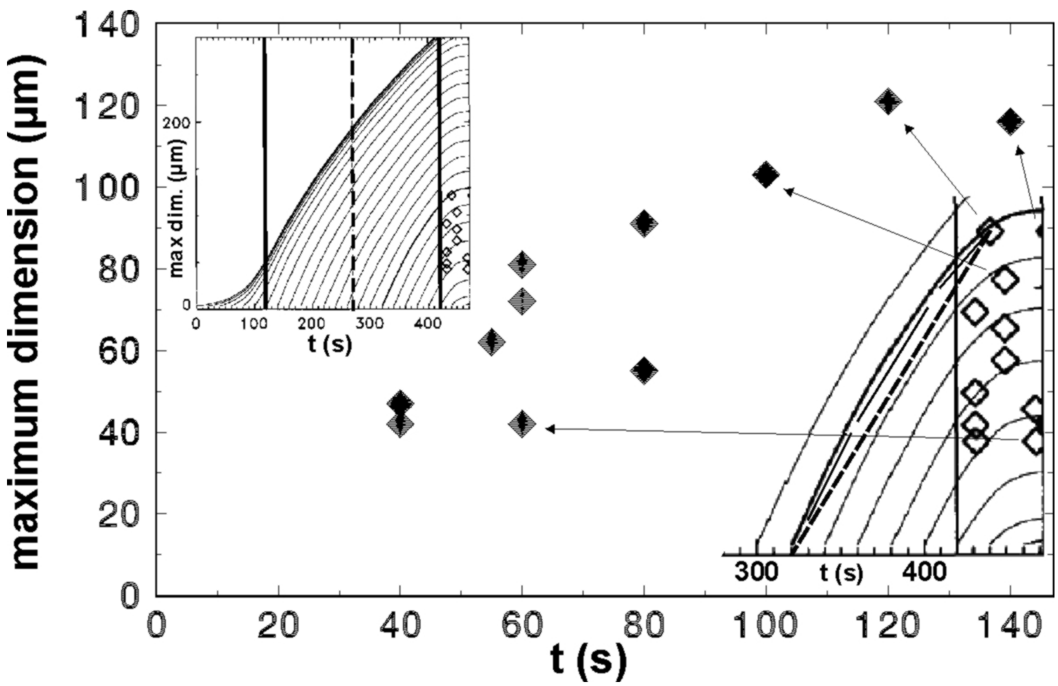

Figure 4. Plot of the particle sizes and estimated growth times in Fe01 (solid diamonds). Top left inset shows possible growth trajectories for wave cloud ice crystals. Lower right inset is an expansion of this figure showing those trajectories for ice crystals detected in the INTACC study.

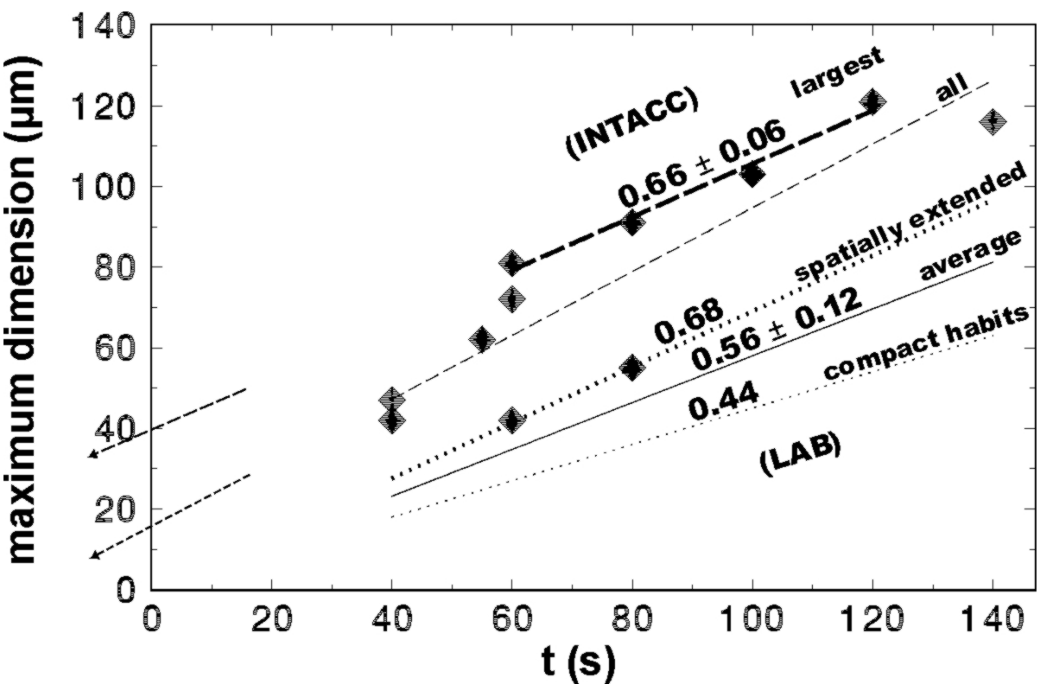

Figure 5. Linear fits of the INTACC crystal growth data (dashed lines) showing a non-zero time axis intercept, along with predicted growth rates from BH04 (solid and dotted lines). Analysis of 2DC instrument response (Baker and Lawson, 2006a) indicates particles are detected at a larger threshold size than assumed by Field et al., resulting in an underestimation of the time of ice crystal nucleation and growth.

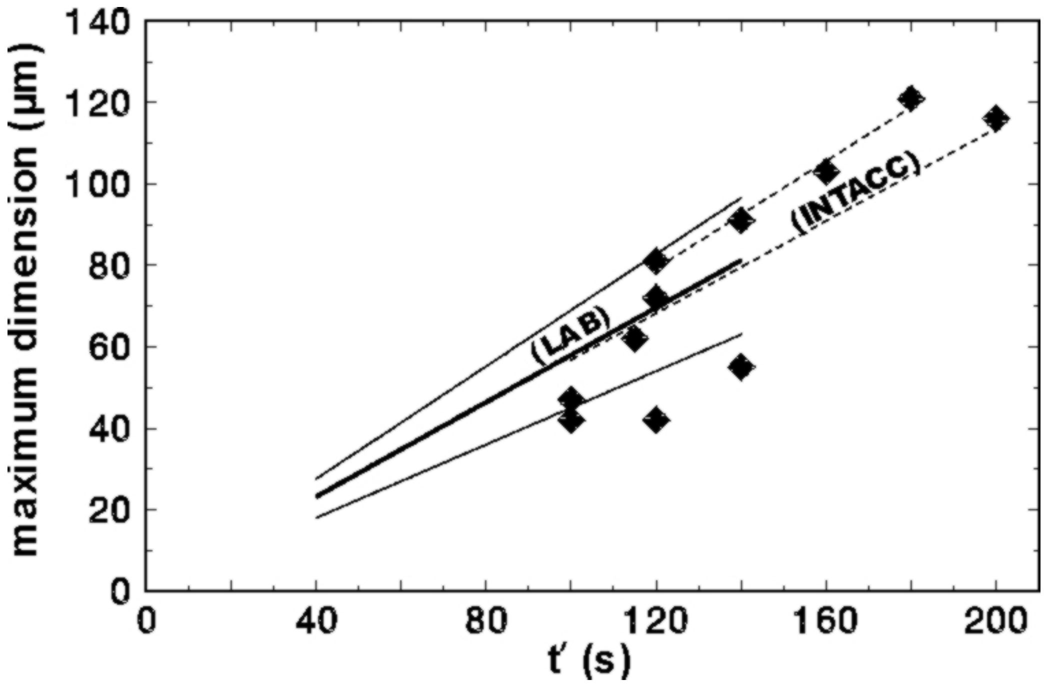

Figure 6. Time shifted results for wave cloud ice particles from slope and 2-DC analysis, along with predicted growth rates from BH04. The time axis above, t´, spans 200 seconds versus 140 second as in figures 4 and 5. The solid lines are the laboratory results for the fastest growing habits (upper line), the habit averaged growth rate (heavier center line), and the slower, less spatially extended habits (lower line). The dashed lines are regression fits of the INTACC data for the largest particles (upper dashed line) and for all the particles (lower dashed line) which is nearly the same as the habit averaged value from the laboratory.

Graphical analysis of the wave cloud ice crystals presented in FE01 clearly indicates an offset with respect to the time axis, i.e. an error in the assumptions about the times of ice crystal nucleation. This is further supported by wind tunnel measurements of the 2-DC size detection threshold (Baker and Lawson, 2006a), hence the time shift applied to the in-cloud data is supported through two independent assessments. It is reasonable to assume that the largest crystals detected in-cloud were those that nucleated first, and/or grew the fastest, and hence are most representative of maximum crystal growth rates. Regardless of the time shift, the growth rates of the largest in-cloud crystals, observed to grow near water saturation, are in good agreement with the laboratory measured values near water saturation, demonstrating that the laboratory results reliably reproduce in situ measurements and observations.

Additionally, laboratory measured projected areas are in agreement with the analysis of over 10^6 ice crystal CPI images by Korolev and Isaac (2003) in terms of roundness or area ratio, the ratio of actual crystal area to a circle of equal maximum dimension. Korolev and Isaac analyzed CPI images from a variety of ice cloud types for temperatures ranging from 0 ^oC to -40 ^oC, and found that crystals exhibited a common behavior with increasing size. As crystals get larger, their roundness decreases, i.e. they become more oblong in terms of shape, or have components which are spatially distributed (e.g. bullet rosettes and rosettes of side planes) such that there are lots of spaces between component structures. The top panels of the figure show the results from Korolev and Isaac, while the middle and bottom panels show the results measured in the laboratory. The laboratory roundness measurements, drawn from a much smaller set of crystals, are nearly identical to those measured by Korolev, especially when adjusted for the mix of habits that occur due to sedimentation in the atmosphere. Korolev and Isaac measured roundness for crystals in clouds where sedimentation of columnar habits from colder overlaying clouds (T< -40 ^{o}C) was often present. Columns and rosettes which have fallen to warmer growth temperatures have larger roundness than at colder temperatures. The opposite is true for clouds with T< -40 ^{o}C (BH09).

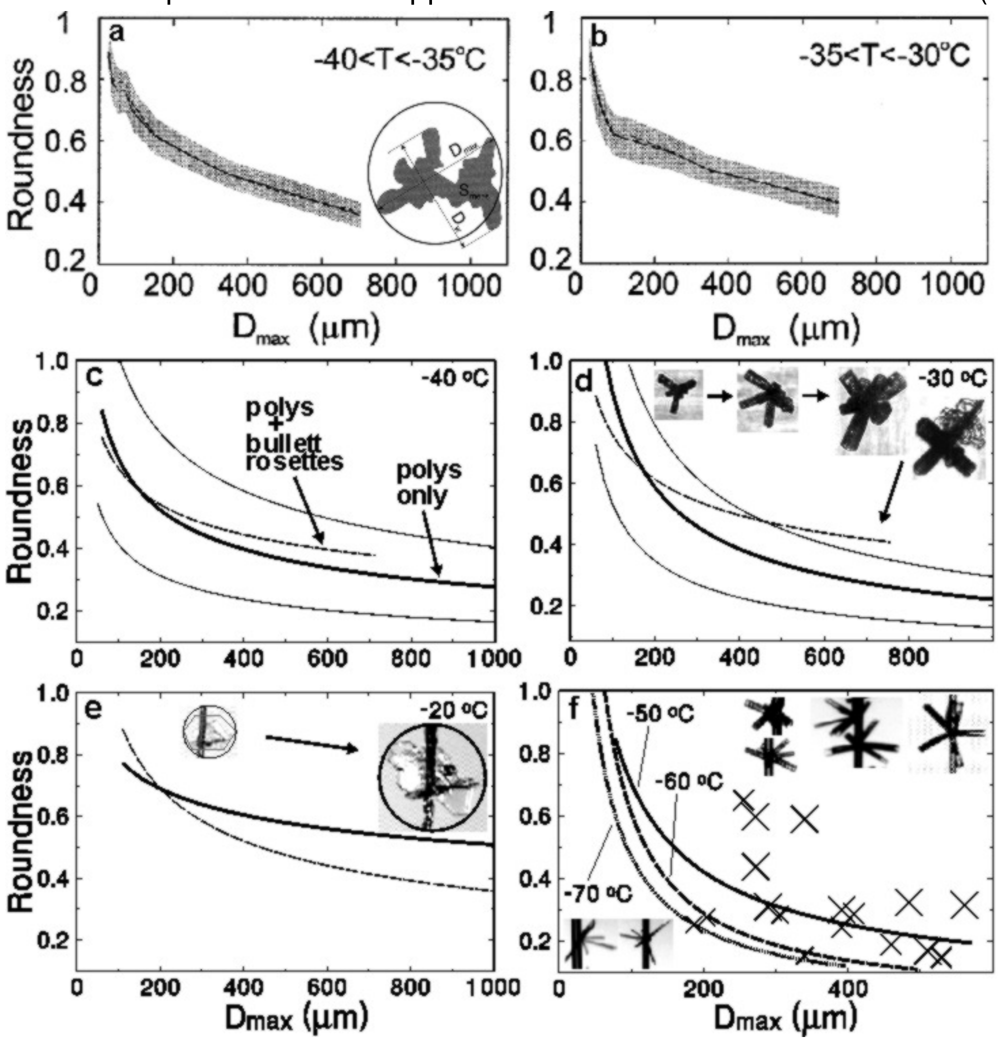

Figure 7. Comparison of "roundness" measured in the laboratory (top graphs) with in situ results measured by Korolev and Isaac (bottom graphs). Small differences are due to the more restricted range of temperatures measured in the laboratory and the inclusion of larger crystal sizes. The two crystals at lower left are the same crystal, initially with a maximum dimension of 300 μm and a roundness of about 0.6, and later with a maximum dimension of 700 μm and a roundness of about 0.45. The “X” symbols in fig. 7-f represent cold rosettes for T< -40 ^{o}C.

Laboratory Measured Growth Rates

Capacitance theories of ice crystal growth have received renewed attention (Westbrook et al. 2008) even though they are unsupported by past laboratory measurements which indicate that capacitance theories over predicts mass growth bya factor of 2 or more (Gonda and Koike, 1982, 1983; Colbeck,1983; Redder and Fukuta, 1989; Takahashi et al., 1991;Nelson and Baker 1996; Fukuta and Takahashi, 1999). This was also the case in Bailey and Hallet (2006). Most of the earlier studies addressed crystal growth for temperatures warmer than -20 ^{o}C using static diffusion chambers or mixing and continuous flow chambers, often for very short growth times (e.g. 45 seconds to a few minutes).

Current capacitance models only describe symmetric hexagonal plates, columns, and bullet rosettes, shapes that constitute a few percent of ice crystals under nearly all atmospheric conditions, with complex polycrystals and asymmetric single crystals dominating habit distributions (Bailey and Hallett, 2009). Also included are the results of Podzimek (1966), experimental measurements of solid and hollow metal hexagonal columns (top line at R = 2.63) which appear to be approximately the same, but this is for hexagonal metal conductors, *not* actual ice crystals. The recent values from WE08 are only slightly higher than those for oblate spheroids and circular cylinders.

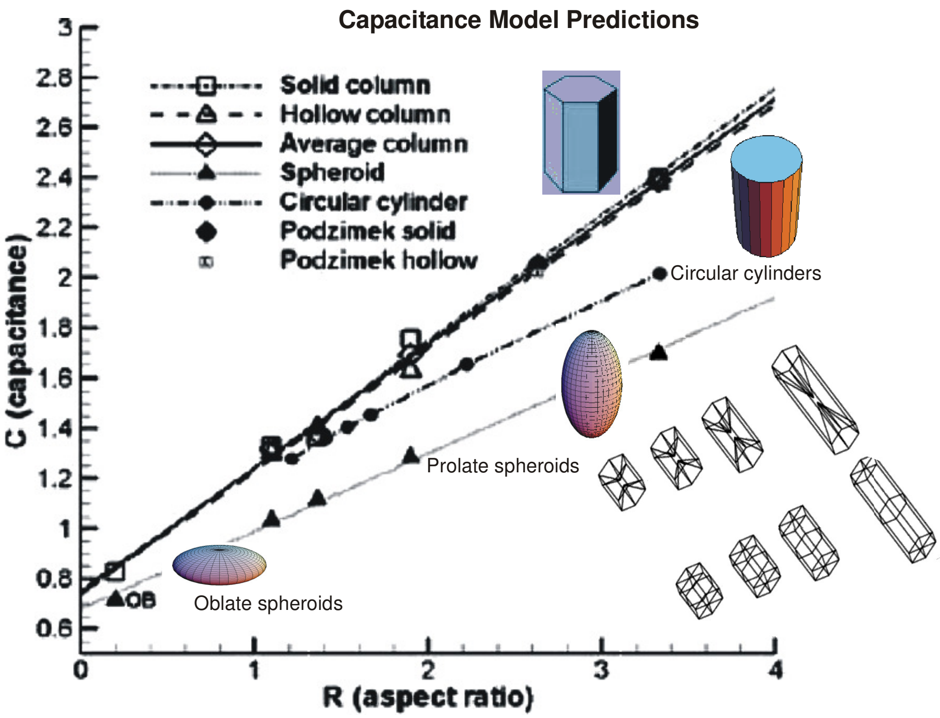

Figure 8. Modeled ice crystal shapes (oblate/prolate spheres and cylinders)and theoretical predicted capacitances versus R, the ratio of crystal axes, c/a, adapted from Chiruta and Wang (2002 and 2005), including their models for solid and hollow hexagonal columns.

Ice Crystals of the Atmosphere

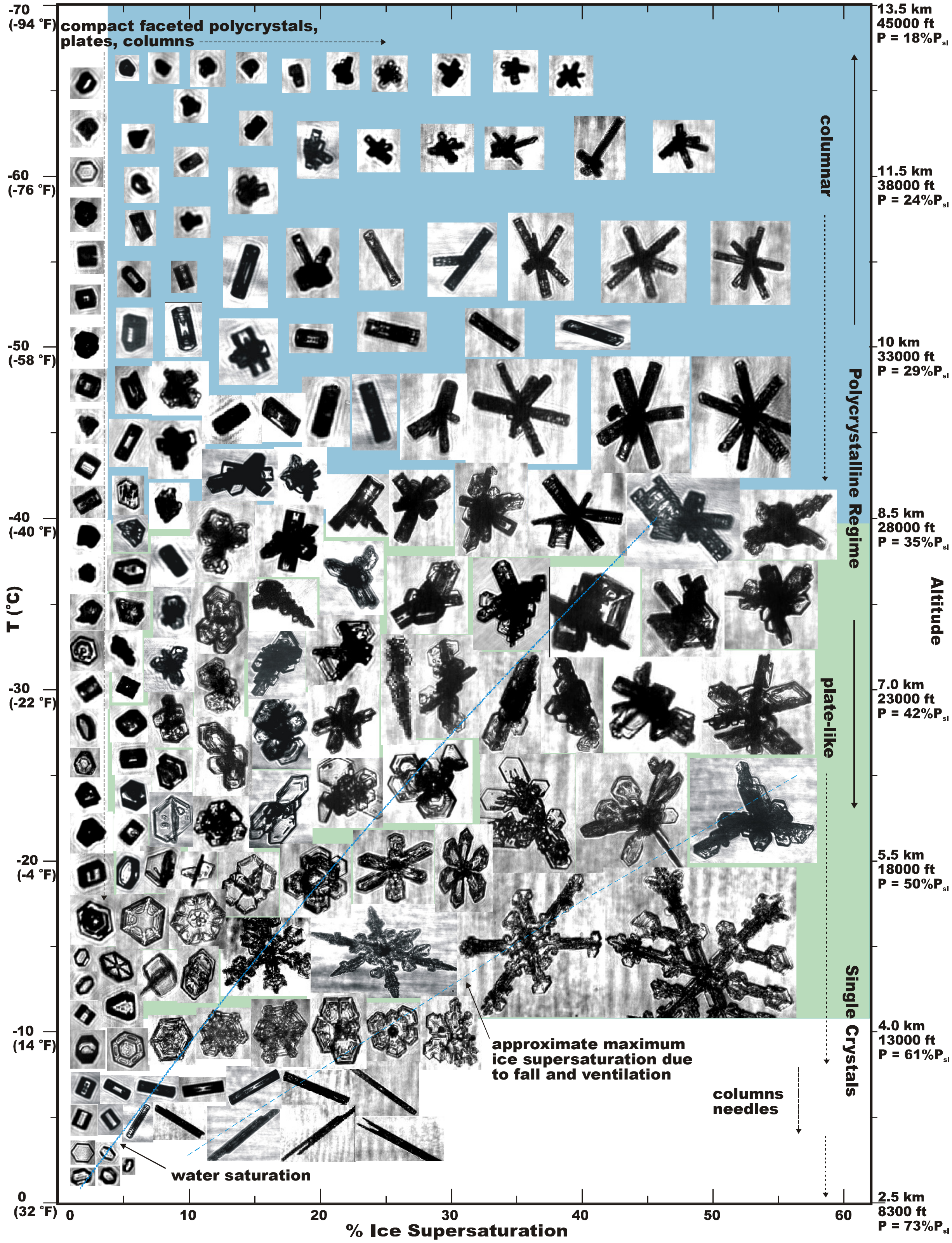

Figure 9. Comprehensive habit diagram adapted from Bailey and Hallett (2009) derived from lab and CPI observations, habits dominated by asymmetric single crystals and polycrystals. Standard atmosphere pressures are given in terms of percent of mean sea level pressure, P_{sl}.

The majority of hexagonal plates and columns observed in situ and in the laboratory have pronounced scalene shapes, irregularly layered facets or steps, and bulk distortions, reflecting the presence of defects that result in non-uniform crystal growth as confirmed with time lapse photography, indicative of non-uniform vapor densities over crystal surfaces, in contradiction to capacitance models.

Figure 10. Images of common in situ plates and columns: a) scalene plates (s) and "flattened" (f) columns in diamond dust; b) acrylic models of columns that are scalene (s) in cross section, resulting in flattened profiles, obviously differing from those of symmetric columns; c) CPI images of plates and columns observed in clouds, revealing rough surfaces, overlapping irregular layers, notches, inclusions, and distorted shapes. In the atmosphere and in the laboratory, pristine symmetric crystals are the exception to the rule.

Westbrook et al. (2008), in discussion of a reportedly improved yet unsubstantiated capacitance model, conclude that a simulation of ice crystal growth, based on particle conditions assumed to be similar to those in BH04, indicated that growth under crowded conditions would result in a reduction of the measured growth rates by a factor of 3. However this is a case of drawing a conclusion from a figure rather than from the text of a paper. This was inferred from images in BH04 and not the description of the strict protocol followed for mass and other growth rate retrievals, the same process that yielded such good agreement with the INTACC comparison of in cloud ice crystal growth that occurred near water saturation, i.e. at high ice supersaturation.

When conducting the growth study, it was obvious that growth rates could be affected by screening effects when crowded crystal conditions were present. Crowding can be avoided with certainty at low ice supersaturation, but becomes progressively more difficult to avoid with increasing ice supersaturation. However there are techniques for nucleation (Bailey and Hallett, 2002) and growth that can be used to control and reduce this problem in many cases. Approximately 100,000 crystals were grown and observed over a few years of concerted laboratory efforts. However, mass and other growth data were retrieved from a small subset of these, approximately 500 crystals, that were assessed to be free from vapor competition or "shadowing" effects. Examples of these retrieval cases are shown in figure 10. Crystals with sizes up to about 700 µm are shown in order to clearly demonstrate habits, but growth data was gathered when the crystals had sizes of 45-300 µm .

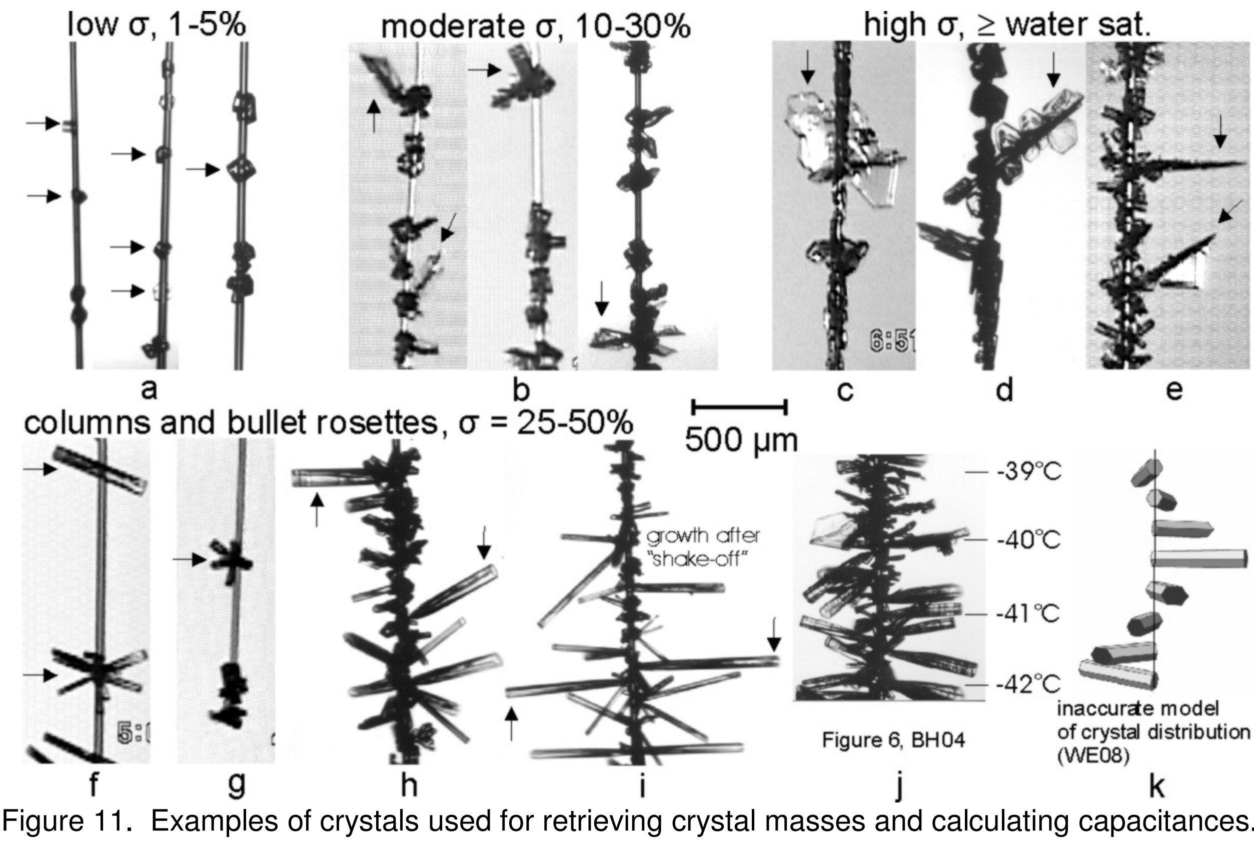

Figure 11. Examples of crystals used for retrieving crystal masses and calculating capacitances. Examples a-i depict cases from which reliable masses were obtained, with arrows indicating candidates for mass retrievals; j and k (WE08) depict cases unsuitable for mass retrieval.

Figure 11-a shows crystals grown at low ice supersaturation where crystal separations of a few to several diameters were easily achieved. Figure 11-b shows crystals grown at moderate ice supersaturation with some crystals growing well away from the substrate, and well separated from neighbors. Figures 11-c to 11-e show crystals grown at high ice supersaturation where the filament eventually became crowded with small crystals. However, even under these crowded conditions, some crystals have grown well away from the crowded substrate. These crystals were the first to nucleate, and they began growing *before* the others had a chance to get started, so initial growth occurred under less crowded conditions, and growth to larger sizes occurred in open space away from the filament, resulting in negligible vapor shadowing. Figures 11-f to 11-i show colder columnar crystals that have grown under similar conditions. Figures 11-j and 11-k depict cases unsuitable for mass retrieval that were not included in this analysis.

Figure 11-k is the misrepresentation of ice crystal distribution presumed by WE08 to represent growth conditions analyzed here, and most closely resembles figure 6 in BH04 (figure 11-j), a crowded growth case shown to demonstrate a temperature dependent habit transition near -40 ^{o}C, from plate-like to columnar habits, which has been confirmed by extensive in situ observations (BH09). The misrepresentation by WE08 placed long columns one crystal diameter apart and rotated 45^{o} with respect to its nearest neighbors, with resulting calculations predicting approximately a 1/3 reduction in mass growth for any "interior" positioned crystal, i.e. one bracketed by neighbors. Crystals chosen for mass retrieval in BH04 and this work typically had at least 3 crystal diameter separations, were rotated 90^{o} or more from neighboring crystals, and were not interior crystals as indicated by arrowed crystals in figure 11. **No growth data was retrieved from crowded growth conditions like those inferred by WE08.**

A number of measures were used to reduce the possible effects of screening. Growth at low ice supersaturations almost always produced well separated crystals through control of nucleation (Bailey and Hallett, 2002). Another simple measure was to restrict mass retrievals to crystals of smaller sizes, typically 45-300 μm in maximum dimension. Hence crystal masses were determined at a size *before* neighboring crystals began to encroach on each other. A method that allowed reliable mass retrievals for some larger crystals at high ice supersaturation involved "shake-off" (figure 11-i). At times when the filament substrate was rotated in order to view crystals at different angles, some weakly attached crystals fell off the filament, leaving large gaps in the crystal distribution. If mass growth was determined from that point onwards for newly isolated crystals, by subtracting initial from final volumes, growth data could be reliably obtained, independent of any screening that may have occurred at an earlier growth stage. Rapid nucleation would sometimes cover the filament with dense compact crystals which resulted in substantial vapor competition, limiting crystals in size and growth, but occasionally, a spatially extended crystal would grow from one of these, extending out into a relatively unobstructed vapor field as seen in figure 11-c,d, and e.

Ice crystal habit is first a function of temperature, with secondary characteristics determined by ice supersaturation, vapor diffusivity, and growth time (particle size). In the laboratory, polycrystalline habits and single crystals exhibit considerable variability from one growth run to the next, even under the same conditions, and vapor shadowing under crowded conditions can affect secondary habit details. So it is important that measures be taken to limit these effects if habits and growth rates representative of those in the atmosphere are to be produced. The fact is if you are patient, and take the time to grow nearly 100,000 crystals, while attempting to control nucleation and limit crowding, statistically, opportunities will present themselves such that reliable growth measurements can be obtained, even under conditions of high ice supersaturation. Proof of this has been demonstrated with agreement observed with the INTACC comparison with respect to maximum dimension growth rates, and roundness comparisons of projected area, agreement that would not occur if growth rates and shapes were reduced or altered by shadowing.

Laboratory Measured Capacitances

Volume and mass growth rates, measured under the same strict protocol previously described, have been used to test the capacitance model of ice crystal growth. A stringent test of capacitance theories has been performed with plates and columns with sizes of 45-300 μm, grown at temperatures between -20 ^{o}C and -70^{o}C, at low ice supersaturation, with sufficiently large crystal separations so as to be free of any vapor competition effects. Results are shown in figure 12 and include fits of predicted capacitances for plates (oblate spheroids) and columns (circular cylinders) from Wang (2002). Theoretical values do not converge at an aspect of one because of the normalization chosen in this study. In computations of theoretical capacitances for symmetric plates and columns, dimensionless values are used in order to simplify calculations. Dimensionless values are obtained by normalizing to the axial length in the basal plane, ***a***, with thickness or height varied (2***c***), and are plotted against the axial or aspect ratio, ***c/a***. In the analysis of crystal shapes from CPI field data and laboratory observations, maximum dimensions and projected areas are typically more meaningful parameters instead of crystallographic axial lengths. The prevalence of irregularly shaped crystals, in addition to the asymmetry exhibited by the majority of plates and columns, negates the relevance of axial ratios when analyzing real ice crystals, with scalene crystals exhibiting at least one long “a” axis and one short “a” axis, and on occasion, six different “a” axes (fully scalene plates), e.g. the two plates labeled “s” near bottom center in figure 10a. Hence normalization in terms of the maximum crystal dimension (plate capacitance to diameter, and column capacitance to length) has been used here in comparison with similarly normalized theoretical values derived from Wang (2002). The laboratory results show that the measured normalized capacitances are lower or considerably lower than the theoretical predicted values in nearly all cases, and no correlation between maximum crystal dimension and capacitance is observed for the size range. Only the measured values for thick symmetric plates, equiaxed crystals (aspect ratio = 1), or very short columns, come close to the theoretically predicted values. In most, but not all cases, symmetric thick plates and short symmetric columns exhibit the largest capacitances. Exceptions to these trends, like the column at -60 ^{o}C with an aspect ratio of 2.6, occur on very rare occasions. Except for results at -20^{o}C, a temperature dominated by the growth of thin plates and plate-like polycrystals, there is also a trend of decreasing capacitance with decreasing temperature, reflecting the decreasing growth rate with temperature shown in figure 2. This decrease in capacitance occurs even as vapor diffusivity increases with decreasing pressure.

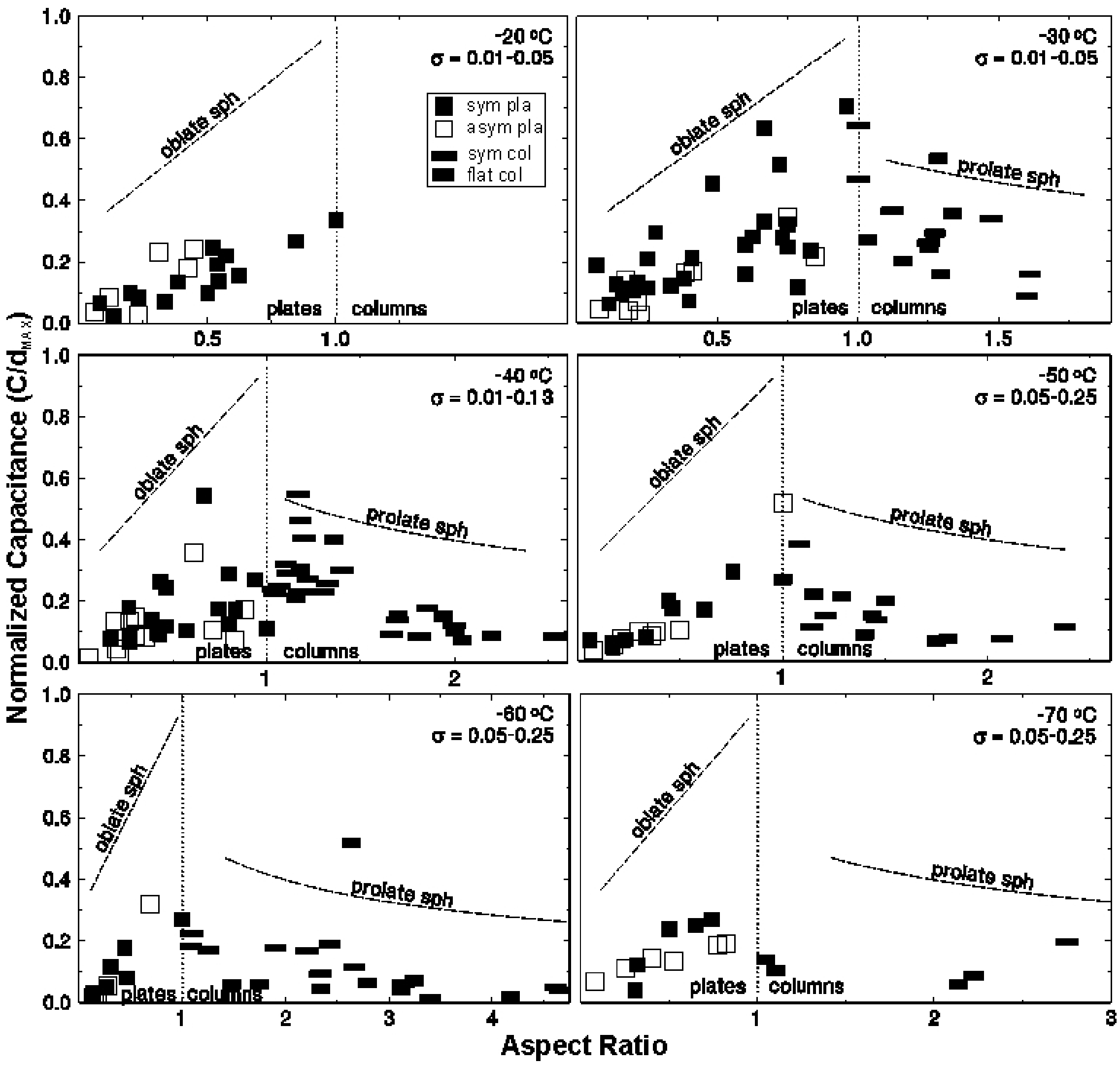

Figure 12. Measured normalized capacitances for plates and columns, normalized to maximum dimension (d_{MAX}), diameter in the case of plates and length in the case of columns, plotted against aspect ratio, length or thickness divided by maximum diameter. Theoretical predictions (dashed curves) have likewise been normalized to maximum dimension and do not converge at an aspect ratio of 1 due to the normalization method as discussed in the text. Solid squares are symmetric plates, open squares are scalene (hexagonally distorted) plates, narrow long rectangles are symmetric columns, and thick rectangles are flattened columns (scalene in cross section). The uncertainty in calculated values is approximately equal to the size of the symbols.

Comparisons of the measured capacitances with symmetric model predictions reveal that in nearly all cases, theoretical values are typically two or more times higher than the measured capacitances, which only rarely come close to the theoretical prediction, and are often considerably smaller, especially at lower growth temperatures. Capacitances of bullet rosettes at higher ice supersaturations also show similar disagreement with capacitance theory predictions. Furthermore, the capacitance calculations of Chiruta and Wang (2005) predict that solid columns and hollow columns have similar mass growth rates, but this is not observed in the laboratory where solid columns have much larger mass growth rates, though only somewhat larger linear growth rates.

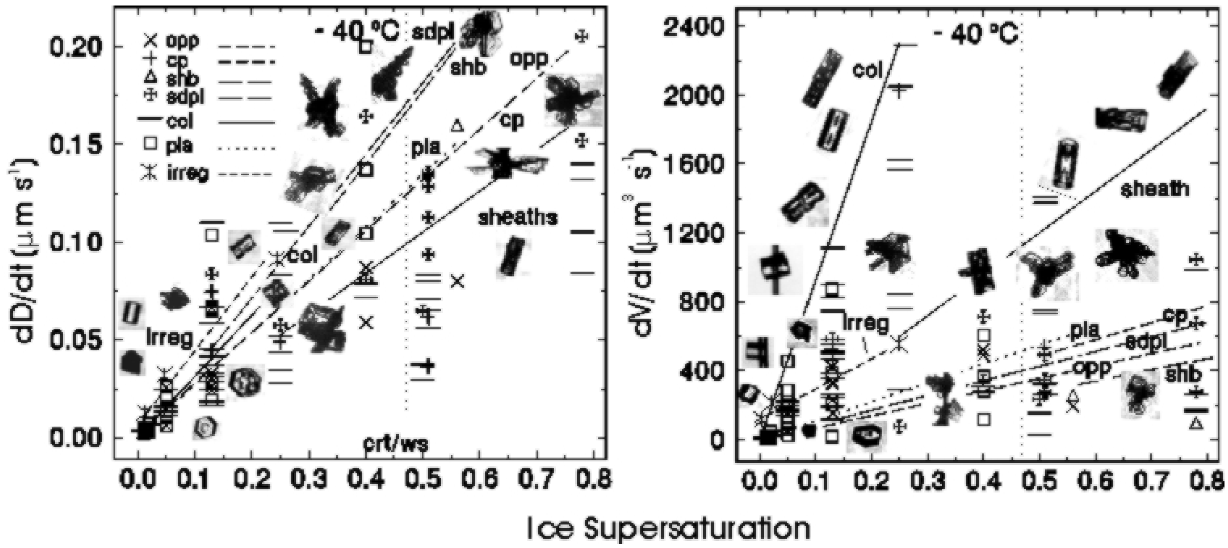

Figure 13. Laboratory measured ice crystal growth rates at -40 ^{o}C for maximum dimension (left) and volume growth (right). Habit designations are the same as in figure 1, -40 ^{o}C being a temperature near the transition from plate-like crystals to columnar forms as shown in figure 9. Solid columns and hollow columns, or “sheaths”, have somewhat similar linear growth rates, but considerably different mass growth rates. An inverse relation between linear and mass growth rates exists for many crystal habits, i.e. spatially extended crystals with large linear growth rates often have mass growth rates that are lower than more compact habits.

All of these results, from low ice supersaturation measurements of plates and columns with no possibility of vapor shadowing effects, to higher ice supersaturation results involving hollow columns, show that the electrostatic analogy of ice crystal capacitance is fundamentally flawed and inadequate for modeling ice crystal growth.

Conclusion

In Bailey and Hallett (2004), growth rates like those shown above have been calculated for specific habits commonly observed in clouds for temperatures between -20 ^{o}C and -70 ^{o}C. These growth rates can be used to determine or predict ice crystal masses for specified growth times, and can be used to calculate mass-to-length and mass-to-projected area ratios of in situ crystals, or for habit ensembles by weighting habit specific growth rates according to habit frequency. This can be done at specific temperatures and ice supersaturations with growth rates that appropriately take these factors into account, unlike current mass-dimensional relations.

Current ice crystal mass estimates applied to in situ observations (Baker and Lawson, 2006, Lawson et al. 2006a & 2006b) are derived from a limited number of in situ mass-dimensional measurements of precipitating single ice crystals collected at the ground (Mitchell et al., 1990; Heymsfield and Kajikawa, 1987). These were often of millimeter size or larger, i.e. generally larger than the mean particle size observed at temperatures below -20 ^{o}C, or often, even the largest in-cloud crystals, excluding aggregates. Crystals collected at the ground have fallen through regimes of increasing temperature, but more importantly, rapidly increasing mass growth rates that typically are not experienced by in-cloud crystals at colder temperatures. If residence times in these varying growth regimes are relatively short, or if ice supersaturations are not too high, falling crystals can essentially retain the shapes they achieved at the colder temperatures where they originated, but will increase in overall mass and effective density (the mass of an ice particle divided by the volume of a sphere of maximum dimension *D* enclosing the particle). This was often observed in the laboratory at the completion of growth runs when chamber plates were allowed to come to nearly the same temperature, resulting in a small residual ice supersaturation, and then allowed to slowly warm together while maintaining a small temperature difference. Over a few hours time, and at low ice supersaturation, crystals were observed to have retained the shapes they had at the end of the growth run, but had obviously become thicker and denser in appearance due an increase in mass. This process will occur in situ at a more rapid rate as ventilated crystals fall through cloudy or clear regions ranging from ice saturation to low or moderate ice supersaturation. Fall at high ice supersaturation leads to relatively rapid modification of habit, indicative of the temperature and habit regimes transited by a falling crystal as demonstrated with bullet rosettes in BH09.

Attempts have been made to statistically manipulate or adjust ground based mass dimensional observations to in-cloud values, first through conversions of original mass-to-length power laws to mass-to-area power laws, followed by integrating particle size distributions (PSD's) according to these estimated masses, and finally comparing this with IWC measurements (Heymsfield et al. 2007; Baker and Lawson, 2006b). IWC measurements obtained with Nevzorov and hot wire probes, chilled mirror and laser hygrometers, have often been shown to have considerable differences when measuring IWC (Schwarzenboeck et al. 2009a and 2009b, Krämer et al. 2009, and Jensen et al. 2009). Estimates of the errors from all these sources, ranging from moderate to substantial, are cumulative, however, the accuracy of these multi-stepped estimates are typically stated in terms of minimization of standard deviations of fits resulting from adjustments of power law coefficients, which is somewhat arbitrary without actual knowledge of true particle masses or effective densities. Results from these multi-stepped manipulations should be presented with a note of caution rather than an air of certainty.

The holy grail of instrumentation for studying in situ ice particles is the development of a nondestructive method for in-cloud collection and measurement of individual particle masses. Until this is developed, laboratory measured growth rates provide the best estimates of in situ ice crystal mass and dimensional growth for particle analysis or models. We state this as a challenge to modelers, and are willing to provide mass and mass dimensional values for such efforts (matt.bailey@dri.edu).

This research was supported by the National Science Foundation, Physical Meteorology Program (ATM-9900560) and NASA (NAGS-7973)

Detailed discussions of the topics in this paper are discussed in two manuscripts publications submitted to JAS;

Ice Crystal Growth Rates: Part 1 - Linear and Area Growth, Confirmation from a Wave Cloud Study and CPI Observations, & Ice Crystal Growth Rates: Part 2 – Mass Growth Rates and the Failure of the Capacitance Model

References:

Bailey, M., and J. Hallett, 2002: Nucleation effects on the habit of vapour grown ice crystals from 2188C to 2428C. *Quart. J. Roy.Meteor. Soc.,* **128,** 1461–1484.

Bailey, M. and J. Hallett 2004: Growth rates and habits of ice crystals between -20 ^{o}C and -70 ^{o}C. *J. Atmos. Sci*. 61, 514-54.

Bailey, M. and J. Hallett, 2006: Measured ice crystal capacitances: the failure of the electrostatic analogy. *12th Conference on Cloud Physics*, 10-14 July 2006, Madison, Wisconsin, P1.59.

Bailey, M. and J. Hallett, 2009: A comprehensive habit diagram for atmospheric ice crystals: confirmation from the laboratory AIRS II, and other field studies. *J. Atmos. Sci*. 66, 2888-2899.

Baker, B. A., and R. P. Lawson, 2006a: In situ observations of the microphysical properties of wave, cirrus, and anvil clouds. Part I: Wave clouds. *J. Atmos. Sci.,* **63**, 3160-3185.
Baker, B. A., and R. P. Lawson, 2006b: Improvement in determination of ice water content from two-dimensional particle imagery. Part I: Image-to-mass relationships. *J. Appl. Meteor. Climatol.,* **45,** 1282–1290.

Chiruta, M. and P.K. Wang, 2002: The capacitance of rosette ice crystals. J. Atmos. Sci. 60, 836-846.

Chiruta, M. and P.K. Wang, 2005: The capacitance of solid and hollow hexagonal ice columns. Geophys. Res.Lett., 32, L05803.

Heymsfield, A. J., A. Bansemer, and C. W. Twhoy, 2007. Refinements to Ice Particle Mass Dimensional and Terminal Velocity Relationships for Ice Clouds. Part I: Temperature Dependence, *J. Atmos. Sci.,* **64**, 1047–1067.

Heymsfield, A. J., P.R. Field, P.J. DeMott, C.H. Twohy, Z. Wang, S.J. Haimov,, D. Rogers, and J.L. Stith, 2010: Ice Particle Development in Orographic Wave Clouds: Results from the Ice In Clouds Experiment. 13th Conference on Cloud Physics, 28 June-2 July 2010, Portland, Oregon.

Jensen, E.J., L. Pfister, T.V. Bui, P. Lawson, B. Baker, Q. Mo, D. Baumgardner, E. M.Weinstock, J. B. Smith, E. J. Moyer, T. F. Hanisco, D. S. Sayres, J. M. St. Clair, M. J. Alexander, O. B. Toon, and J. A. Smith, 2008: Formation of large (≈ 100μm) ice crystals near the tropical Tropopause. *Atmos. Chem. Phys*., **8**, 1621–1633.

Krämer, M., C. Schiller, A. Afchine, R. Bauer, I. Gensch, A. Mangold, S. Schlicht, N. Spelten, N. Sitnikov, S. Borrmann, M. de Reus, and P. Spichtinger, 2009: Ice supersaturations and cirrus cloud crystal numbers. *Atmos. Chem. Phys*., **9**, 3505–3522.

Korolev, A.V. and G.A, Isaac, 2003: Roundness and aspect ratio of particles in ice clouds. *J. Atmos. Sci.* **60**, 1795-1808.

Schwarzenboeck, A, G. Mioche, A. Armetta, A. Herber, and J.-F. Gayet, 2009a: Response of the Nevzorov hot wire probe in clouds dominated by droplet conditions in the drizzle size range *Atmos. Meas. Tech*., **2**, 779–788.

Schwarzenboeck, A, G. Mioche, A. Armetta, A. Herber, and J.-F. Gayet, 2009b: Response of the Nevzorov hot wire probe in Arctic clouds dominated by very large droplet sizes. *Atmos. Meas. Tech. Discuss*., **2**, 1293–1320.

Wang, Pao K., 2002: Shape and microdynamics of ice particles and their effects in cirrus clouds. *Advances in Geophysics*, Vol 45. Renata Dmowska and Barry Saltzman, editors. Academic Press, San Diego pp. 1-252.

Westbrook, C. D., R. J. Hogan, and A. J. Illingworth, 2008: The capacitance of pristine ice crystals and aggregate snowflakes. *J. Atmos. Sci*., 65, 206219.